Optical antennas based on coupled nanoholes in thin metal films

Y. ALAVERDYAN*†, B. SEPÚLVEDA*, L. EURENIUS, E. OLSSON AND M. KÄLL†

Department of Applied Physics, Chalmers University of Technology, SE-412 96 Göteborg, Sweden

*These authors contributed equally to this work

†e-mail: yury@fy.chalmers.se; kall@fy.chalmers.se

Published online: 18 November 2007; doi:10.1038/nphys785

The ability to control optical effects at the nanoscale is a challenge that could be of great importance for a range of photonic applications. However, progress requires a deep understanding of the relationship between near-field and far-field properties of the individual elements of the nanostructure, as well as of the role of nano-optical interactions. Here, we show that the strong interaction between nanoholes in optically thin metal films can be used to readily tune their spectral response and visibility. Control of this interaction in short chains of nanoholes enables either amplification or almost total suppression of the scattered light. The phenomena are interpreted in terms of hole coupling mediated via antisymmetric surface plasmon polaritons, which makes the nanohole chains effectively behave as linear wire antennas.

The possibility to control light at the nanoscale through the use of surface plasmons has attracted great attention to the plasmonics field over the past few years. The interest originates in the unique optical properties of metallic nanostructures, which allow the diffraction limit present in conventional optics to be surpassed[1]. Combined with the electrical properties of metallic nanostructures, plasmonics may also pave the way to the merging of electronics and photonics at the nanoscale[2]. The progress in plasmonics, which has been supported by recent advances in nanofabrication techniques and electrodynamics theory, has led to the discovery of a variety of nano-optical effects[3–5] and the proposition of a range of novel applications in areas such as integrated nanophotonic circuits[6], optical antennas[7,8], spectroscopy[9], sensing[10–12] and metamaterials[13–16].

During the past decade, particular attention has been devoted to the properties of nanoscopic apertures in optically thick metal films, for which a combination of surface plasmon and diffractive coupling effects, together with localized shape resonances, gives rise to extraordinary optical transmission phenomena[3,17–25]. Here, we investigate the optical properties of linear chains of nanoholes in optically thin gold films. Such films are characterized by surface plasmons of very short wavelength, of the order of half the optical vacuum wavelength of light or less, as well as charges of the same sign aligned across the metal film[26]. We show that the surface plasmons emitted by a given nanohole strongly modify the charge distribution around its nearest neighbours, which leads to drastic changes in their scattering characteristics. This interaction can be exploited to control the spectral response and visibility of finite hole chains. The essence of the phenomenon is shown in Fig. 1, which shows dark-field microscopy images of two orthogonal chains of nanoholes milled in a 20 nm thin gold film. Depending on the direction of illumination, the scattering from one of the chains is strongly amplified, whereas the perpendicular chain completely disappears. The effect of amplification or disappearance of the light scattered by the chains is a result of the interaction between the nanoholes and the coherent superposition of their far-field radiation patterns. To understand this interaction, and gain control over the optical response of the chains, we analyse their elastic scattering spectra for different numbers of nanoholes and for different separation distances between the holes.

ELASTIC SCATTERING SPECTRA

Because the gold films of thickness $t = 20$ nm are partially transparent and the nanohole density is very low, we cannot carry out standard transmission measurements to characterize the spectral properties of the hole chains. Instead, we measure elastic scattering spectra using an inverted dark-field microscope. There are four experimentally accessible scattering configurations that are compatible with the linear symmetry of the chains, that is, the projection of the incident wavevector (k) in the plane of the sample can be oriented either parallel or perpendicular to the chains and, for each of these two cases, the polarization of the incident light can be parallel or perpendicular to the chains. We begin by analysing the cases where k is perpendicular to the chains, which corresponds to a situation where all nanoholes in a chain are excited in phase, see Fig. 2. The nanoholes were about $D \approx 70 \pm 10$ nm in diameter. Results are shown for chains with $N = 2$ and $N = 8$ for edge-to-edge separation distances (d) between 30 and 390 nm. As a reference, the lowest trace in the first column (Fig. 2a) shows the spectrum for one isolated nanohole. In accordance with previous studies[27,28], the single-hole spectrum has a lorentzian line shape with a resonance wavelength of $\lambda_0 \approx 680$ nm. In contrast, the nanohole pairs exhibit a strong polarization-dependent modulation of the scattering peak position and intensity as a function of separation distance. The variation is most pronounced when the polarization is parallel to the pair axis (Fig. 2a). For the shortest edge-to-edge distances, $d = 30$–60 nm, the peak is weak and blue-shifted compared with the single-hole resonance, but a gradual red-shift and intensity enhancement occurs when the distance between the nanoholes increases. Interestingly, the scattering intensity per nanohole is amplified by approximately ten times when it reaches the maximum

at $d \approx 150$ nm (see Fig. 2a). For longer distances, the red-shift continues, intensity decreases and the peak almost completely vanishes at $d \approx 300$ nm. When the distance is further increased, a second dispersing scattering peak emerges from the blue side of the spectrum. As shown in Fig. 2a, the same kind of spectral evolution, but even more pronounced, is seen for the $N = 8$ chain in the parallel polarization configuration. Turning to the perpendicular polarization configuration, Fig. 2b, a much weaker spectral variation with respect to a single hole is observed, although we note that the peak is strongly red-shifted for the shortest edge-to-edge distances.

COUPLED-CHARGE SIMULATIONS

To understand the reason for the observed spectral variations, the nature of the optical excitation of a single nanohole and the coupling of adjacent holes through the surrounding metal film have to be considered. As recently discussed[27], electrodynamics simulations show that the single-hole resonance can be assigned to a localized surface plasmon (LSP) of electric dipole character. Thus, the incident optical field polarizes the nanohole and induces an electric dipole moment $\mathbf{P} = \alpha(\omega)\mathbf{E}_0$ oriented parallel to the incident polarization vector $\mathbf{E}_0$. To obtain a qualitative analytical expression for the frequency-dependent polarizability of a nanohole, we use the Clausius–Mossotti relation $\alpha = r^3(\varepsilon_S - \varepsilon_M)/(\varepsilon_S + 2\varepsilon_M)$ for a small spherical vacuum void ($\varepsilon_S = 1$) of radius r in a metal characterized by a Drude dielectric response $\varepsilon_M(\omega) = 1 - \omega_p^2(\omega(\omega + i\gamma))^{-1}$, where ω_p is the plasma frequency and γ^{-1} is the dephasing rate of the free electrons. This yields a lorentzian polarizability $\alpha(\omega) = \alpha_0\omega_0^2/(\omega_0^2 - \omega^2 - i\omega\gamma)$, with $\alpha_0 = -r^3/2 < 0$ and $\omega_0 = \sqrt{(2/3)}\omega_p$, which is comparable to the case of a small metal particle in vacuum, for which $\alpha_0 = r^3 > 0$ and $\omega_0 = \sqrt{(1/3)}\omega_p$. Analogous to the case of Au nanodiscs, the disc-like nanoholes considered here exhibit a red-shifted LSP resonance $\omega_0 < \sqrt{(2/3)}\omega_p$, corresponding to charge oscillations in the plane of the metal film, and a larger linewidth $\Gamma > \gamma$ due to radiative losses[28,29]. However, two crucial differences distinguish nanoholes from nanodiscs, that is, the sign of the d.c. polarizability α_0 and the fact that the nanohole LSP can decay through surface plasmon polariton (SPP) emission[27]. These observations constitute the cornerstones for understanding and controlling the interaction of nanoholes in optically thin gold films.

For small distances between holes or discs ($d < D$), we expect an essentially electrostatic coupling that can be analysed through the coupled-dipole equation (CDE): $P_i = \alpha_i E_0 - \alpha_i A_{ij} P_j$ (ref. 30). The CDE states that the net dipole moment at position i is induced by the coherent sum of the incident field E_0 and the fields from all other dipoles $A_{ij}P_j$. The electrostatic propagator A_{ij} simply equals $-2/d^3$ for incident polarization parallel to the axis connecting the dipoles and $1/d^3$ for the perpendicular case. By assuming two equal dipoles, described by the lorentzian polarizability $\alpha(\omega)$ above, it is easy to solve the CDE to find the two corresponding renormalized resonance frequencies $\tilde{\omega}_\parallel = \omega_0\sqrt{1 - 2\alpha_0/d^3}$ and $\tilde{\omega}_\perp = \omega_0\sqrt{1 + \alpha_0/d^3}$. For holes or voids, for which $\alpha_0 < 0$, we thus expect a blue-shift ($\tilde{\omega}_\parallel > \omega_0$) for the parallel polarization configuration and a red-shift ($\tilde{\omega}_\perp < \omega_0$) for the perpendicular polarization case. This is in qualitative agreement with the spectral shifts observed for small edge-to-edge distances d in Fig. 2 and is opposite to the well-known case of two interacting discs[31] ($\alpha_0 > 0$).

For larger distances ($d > D$), the importance of the electrostatic coupling diminishes and holes, as well as discs, will interact through propagating retarded waves. In the case of holes in an optically thin metal film, the dominant part of this interaction is due to emission of antisymmetric bound SPPs (a_b modes)[27,28,32]. As shown schematically for a nanohole pair in Fig. 3b, each hole

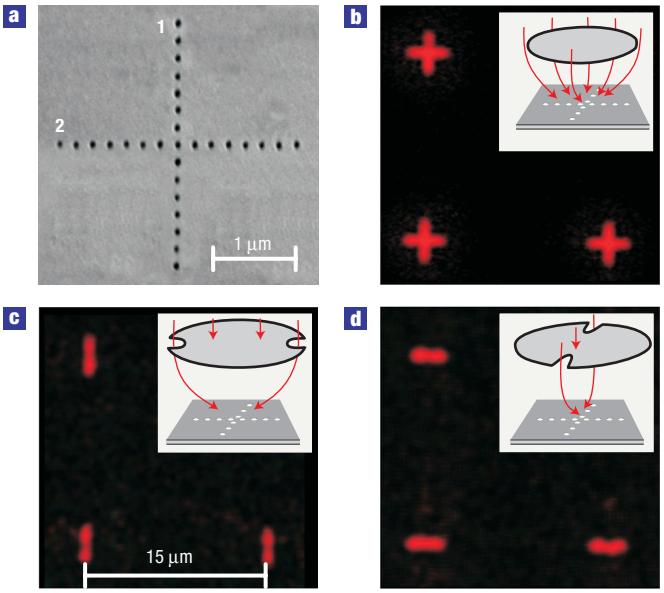

Figure 1 Illustration of visibility phenomena in two orthogonal nanohole chains. **a**, Scanning electron microscopy image of two orthogonal chains of 80-nm-diameter nanoholes with 150 nm edge-to-edge separation distance. **b–d**, Dark-field microscopy image of orthogonal chains of nanoholes for unpolarized illumination incident at an angle of $62.5^\circ \pm 10^\circ$ from all of the directions (**b**), the direction of incidence perpendicular to the nanohole chain **1** (**c**) and perpendicular to the nanohole chain **2** (**d**).

in a chain acts as an efficient source of SPPs that are emitted preferentially in the direction of the induced dipole moment $\mathbf{P}$ (refs 27,33). If the holes are illuminated in-phase and the edge-to-edge distance between adjacent nanoholes fulfils the criterion $d = (n + 1/2)\lambda_{SPP}$, $n = 0, 1, 2$ and so on, where λ_{SPP} is the wavelength of the a_b mode, then the charge induced by the incident light and the surface charge due to SPP emission adds up at the hole edges. As a consequence of this matching, the induced dipolar charges at each nanohole increase, which results in a large amplification of the scattering intensity. Likewise, for $d = n\lambda_{SPP}$, $n = 1, 2, \ldots$, we expect a suppression of the scattering intensity due to a partial cancellation of the primary induced charge by the SPP charge wave. This scenario can be formulated in terms of a coupled-charge equation, which is simpler than, but analogous to, the CDE[30]. We thus express the total charge at the edge of one hole as the sum of an induced charge and a charge due to SPPs emanating from the nearest edge of a neighbouring hole, that is, $q_n = \alpha(\omega)E_0/D + cq_{n-1} \cdot \exp(ik_{SPP}d)$ for the case of in-phase illumination, where $c < 1$ is a coupling constant and $k_{SPP} = 2\pi/\lambda_{SPP} + i/\delta_{SPP}$ is the complex wavenumber of the a_b mode, with δ_{SPP} being the decay length. For an infinite chain, we have $q_n = -q_{n-1}$ and the solution of the coupled-charge equation can be expressed in terms of a renormalized polarizability: $\tilde{\alpha}(\omega) = \alpha(\omega)/(1 + c \cdot \exp[ik_{SPP}d])$. The scattering cross-section for a hole can then be evaluated from:

$$\sigma_s \propto \omega^4|\tilde{\alpha}(\omega)|^2 = \frac{\omega^4|\alpha(\omega)|^2}{1 + \tilde{c}^2 + 2\tilde{c} \cdot \cos(2\pi d/\lambda_{SPP})}, \qquad (1)$$

where $\tilde{c} = c \cdot \exp[-d/\delta_{SPP}]$. To simulate the resulting scattering spectra, we need to evaluate the dispersion relation $\omega(k)$ of the a_b mode[34]. Figure 3c shows a calculation of the wavelength and the decay length for a 20 nm gold film on glass in air obtained using the

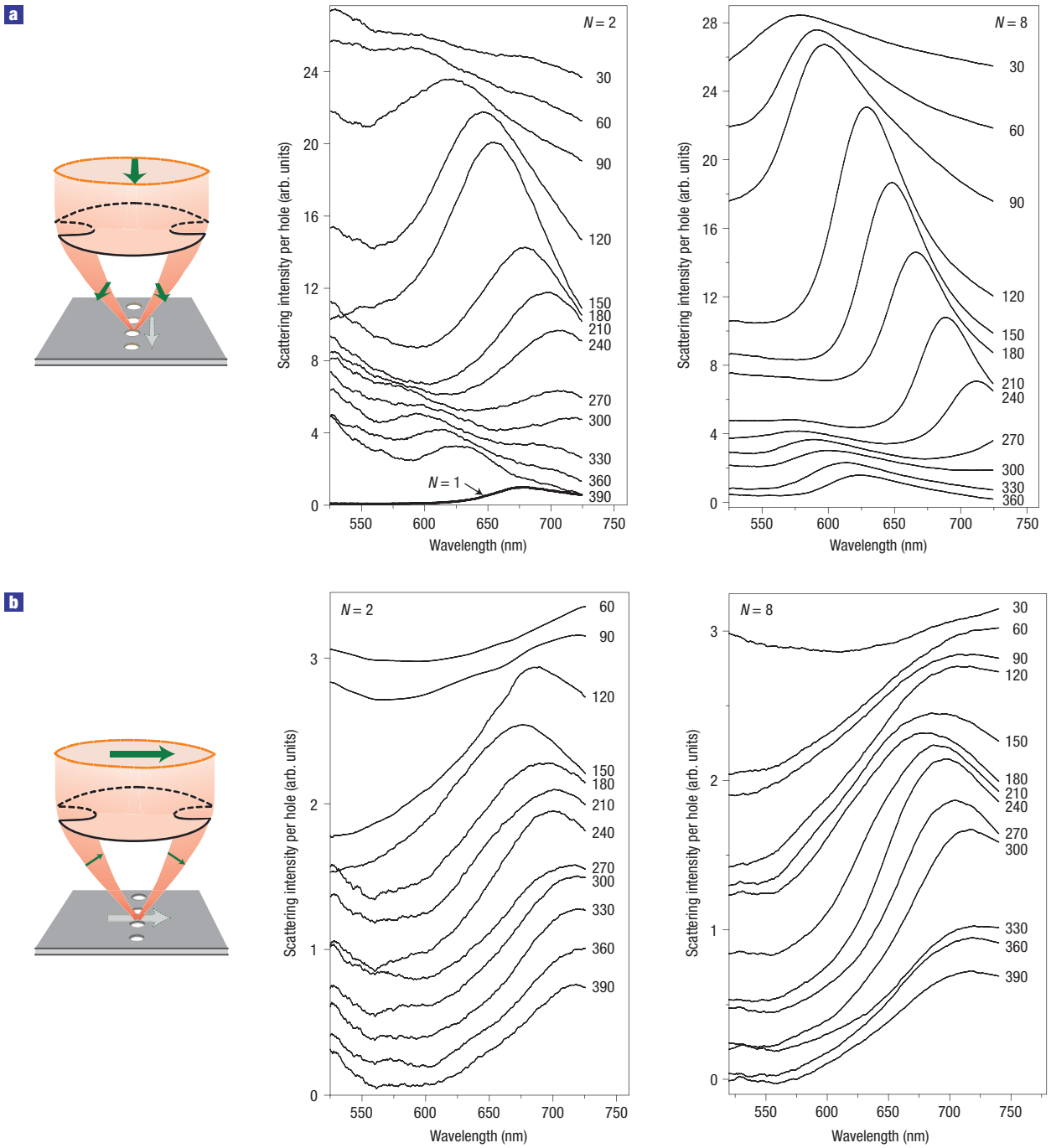

Figure 2 Experimental elastic scattering spectra of nanohole chains ($N = 2, 8$) measured in the in-phase configuration of incidence. a,**b**, Polarization parallel (**a**) and perpendicular (**b**) to the chain (configurations of incidence are shown to the left). The diameter of the single nanohole is about 80 nm. The diameter of the nanoholes in $N = 2$ and $N = 8$ chains is about 75 and 65 nm, respectively.

transfer-matrix formalism[34]. Owing to the strong coupling between the two metal surfaces in the optically thin film, the a_b mode is strongly dispersive compared with the light lines $\omega = ck$ of the surrounding dielectrics. Hence, the wavelength of the a_b mode turns out to be only of the order of half the vacuum wavelength λ_0 within the spectral range of interest. This is in contrast to the case of the symmetric leaky mode, the other SPP mode allowed in the thin film, for which λ_{SPP} is only marginally smaller than λ_0 (ref. 27).

Figure 3a shows simulated scattering spectra based on equation (1) for an infinite chain of nanoholes, a lorentzian polarizability $\alpha(\omega)$ that reproduces the experimental single-hole spectrum, and the calculated values of λ_{SPP} and δ_{SPP}. To account for the spectral shifts at small distances, we use the 'electrostatic' resonance positions $(\tilde{\omega}_{\parallel}, \tilde{\omega}_{\perp})$ with $\alpha_0 = -3.5 \times 10^4\,\mathrm{nm}^3$. Using a single adjustable coupling parameter ($c = 0.8$), the simple model clearly captures the essential features of the hole–hole

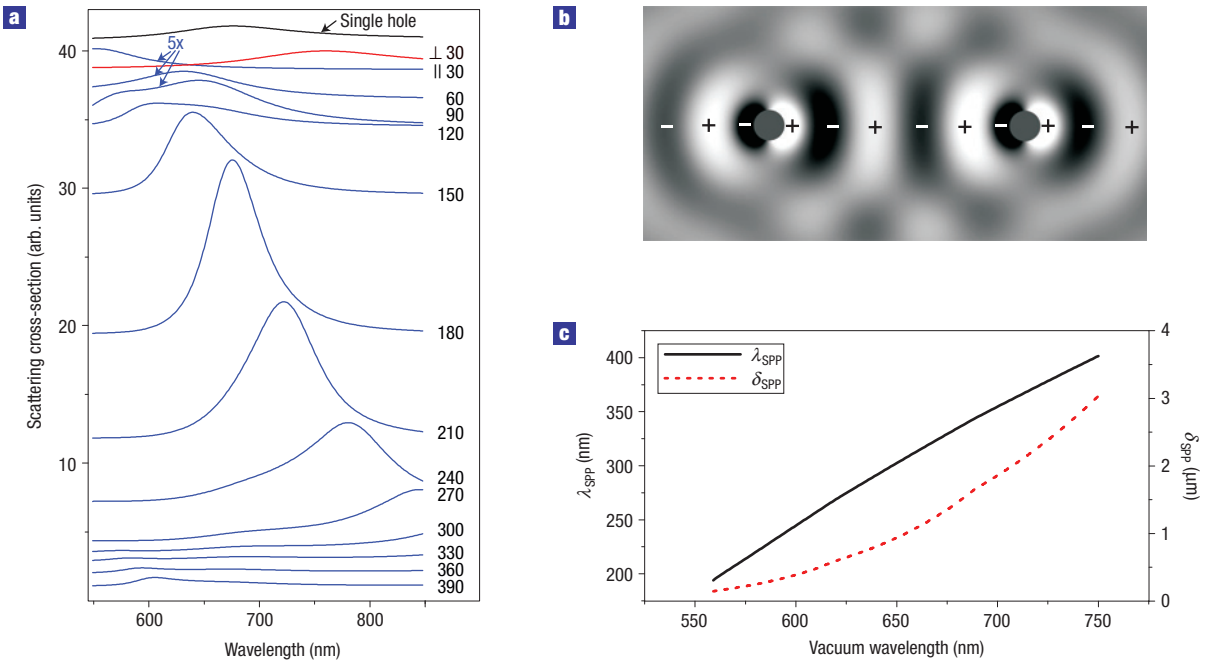

Figure 3 Model of hole–hole interaction mediated by the antisymmetric bound (a_b) SPP mode. a, Model calculations of scattering spectra versus edge-to-edge distance for an infinite chain of holes using the coupled-charge equation. **b**, Schematic diagram of the top view of two nanoholes interacting via SPP emission. **c**, SPP wavelength and decay length of the a_b mode versus vacuum wavelength for a 20 nm Au film on glass in air.

interaction: a red-shift of the scattering peak with increasing separation distance, a large enhancement of the scattering intensity at $d = \lambda_{SPP}/2$, a minimum of the scattering intensity at $d = \lambda_{SPP}$ and the appearance of a second peak in the short-wavelength spectral region for $d > \lambda_{SPP}$. Because the optimum hole separation involves an SPP propagation distance of $\sim\lambda_{SPP}/2$, the propagation losses are low ($\sim$15% at 650 nm, see Fig. 3c).

In the case of the perpendicular polarization, the surface charge waves with maximum amplitude propagate perpendicular to the chain axis. As a consequence, the nanoholes are weakly coupled, and the change of the separation distance only slightly affects the scattering spectrum of the chains, except for the shortest distances where the electrostatic interaction induces the red-shift (Figs 2b and 3a).

OPTICAL NANO-ANTENNAS

In the previous paragraphs, we focused on the spectral evolution for the cases when the nanohole chains were illuminated in-phase. We now investigate the out-of-phase illumination configuration and try to quantify the invisibility phenomenon shown in Fig. 1. Figure 4b shows a comparison of the scattering spectra measured in the two configurations (Fig. 4a) for chains containing different numbers of nanoholes. The polarization and separation distance was chosen to maximize the scattering intensity for the in-phase case (that is, polarization parallel to the chains and $d = 150\,\text{nm} \approx \lambda_{SPP}/2$, see Supplementary Information for the case of perpendicular polarization). As anticipated from the results shown in Fig. 2, we observe a rapid increase in intensity for the in-phase configuration with increasing N. In contrast, the scattering intensity in the out-of-phase configuration decreases as the number of nanoholes in the chain increases and already at $N = 3$ there is an order-of-magnitude difference in integrated intensity between the two configurations (Fig. 4b). The variation in peak height with d for $N = 3$ is shown in Fig. 4c. We find a rapid divergence between the two configurations for $d < \sim$400 nm, again with maximum contrast at $d \approx \lambda_{SPP}/2$.

To understand and quantify the invisibility phenomenon, we need to delineate the differences in excitation and collection efficiency between the different illumination configurations. Starting with the excitation process, we first evaluate how the effective polarizability of a hole inside a chain varies with angle of incidence θ. We assume a p-polarized wave with the surface projection of the incident k vector parallel to the chain, that is, $k_{\parallel} = k\sin(\theta)$. The case $\theta = 0$, that is, normal incidence, thus simulates the case when all holes in a chain are excited in-phase, whereas $\theta \approx 60°$ simulates the out-of-phase configuration shown in Fig. 4a. By inserting the appropriate phase factors $\exp[i\mathbf{k}_{\parallel} \cdot \mathbf{r}]$ for the incident field into the coupled-charge equation, we obtain the ratio:

$$\frac{|\tilde{\alpha}(\theta)|^2}{|\tilde{\alpha}(0)|^2} = \frac{1 + \tilde{c}^2 - 2\tilde{c}\cos[(k_{SPP} - k\sin(\theta))d]}{1 + \tilde{c}^2 - 2\tilde{c}\cos[k_{SPP}d]}, \qquad (2)$$

where $|\tilde{\alpha}(0)|^2$ is given by equation (1). Inserting $d = \lambda_{SPP}/2$, we find $|\tilde{\alpha}(\theta)|^2/|\tilde{\alpha}(0)|^2 = [1 - (4\tilde{c}/(1+\tilde{c})^2)\sin^2(kd\sin(\theta))] < 1$. Equation (2) thus predicts a reduction in effective polarizability with angle, resulting in an 'excitation lobe' that is narrower than for a chain of uncoupled holes ($c = 0$). This antenna effect is due to the SPP coupling and is a consequence of the imperfect constructive interference between the primary induced charge and the SPP charge originating from a neighbouring hole edge that occurs for out-of-phase illumination. However, the effect is not very large: for the parameters used previously, we find that $|\tilde{\alpha}(\theta)|^2/|\tilde{\alpha}(0)|^2 \approx 0.6$ within the wavelength range of interest, which is obviously far from the almost complete intensity suppression seen in Fig. 4.

We now turn to the emission process, and investigate whether a further reduction in intensity can be expected due to the fact

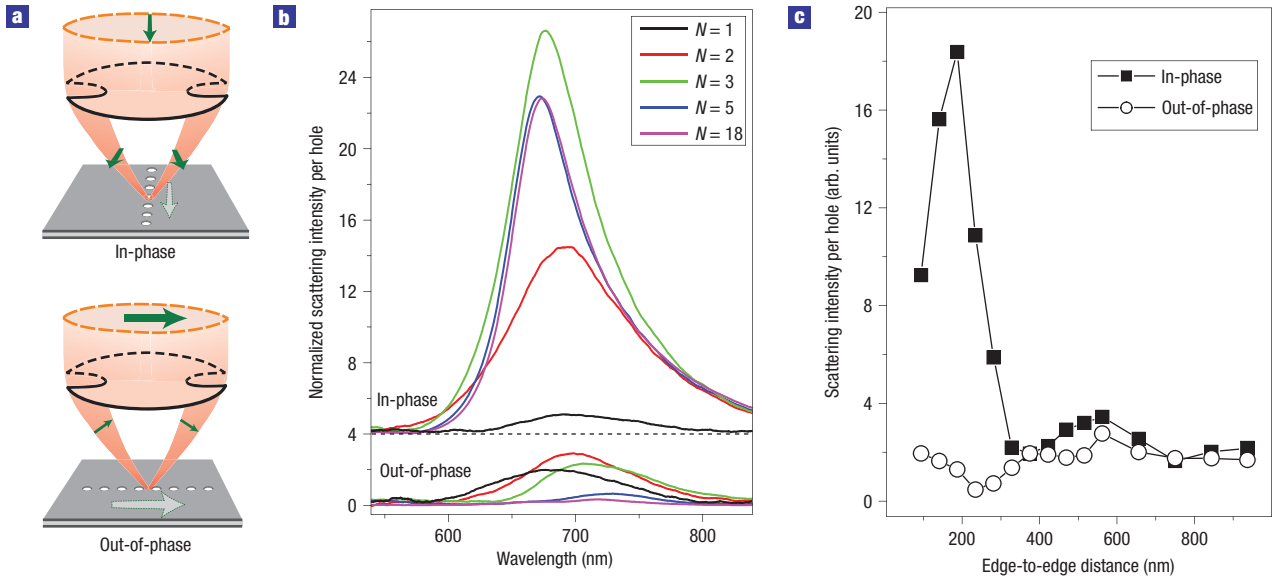

Figure 4 Comparison of experimental elastic scattering spectra for the in-phase and out-of-phase configurations for different numbers of nanoholes. a, Schematic diagrams of the in-phase and out-of-phase illumination configurations for polarization parallel to the chain. **b**, Experimental elastic scattering spectra for chains containing different numbers of nanoholes ($N = 1$–18). **c**, Experimental elastic scattering intensity dependence on the edge-to-edge distance between nanoholes (d) for the $N = 3$ chain in the in-phase and out-of-phase illumination configurations. The diameter of all nanoholes is about 80 nm.

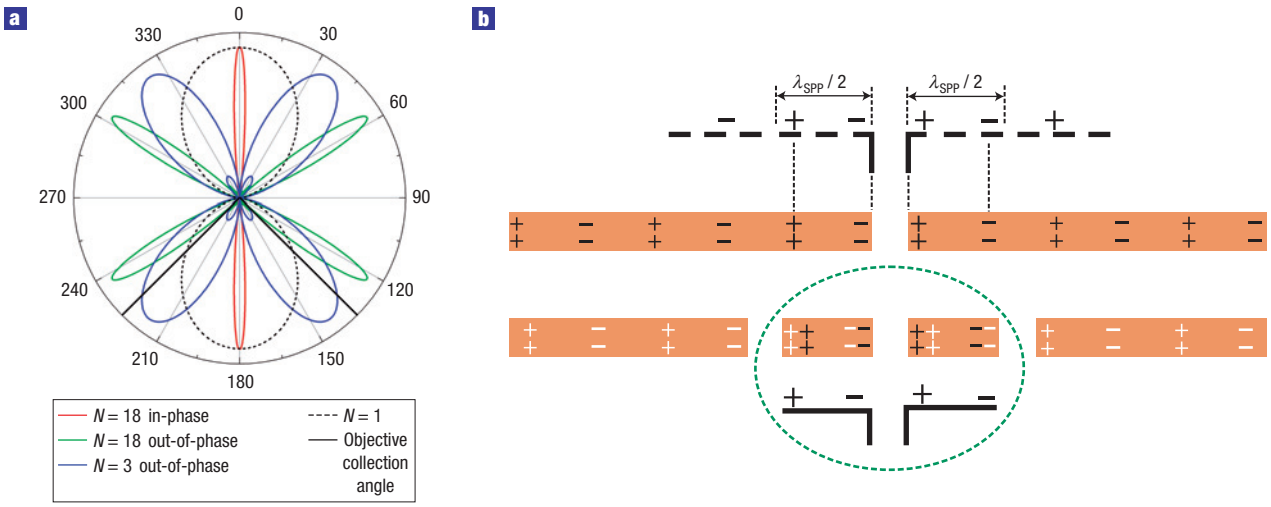

Figure 5 Nano-antenna based on a chain of nanoholes. a, Calculated far-field emission patterns for a linear chain of uncoupled point dipoles ($N = 1$–18) for the in-phase and out-of-phase configurations. **b**, Schematic analogy between the charge distribution in nanohole chains and conventional wire antennas: (from the top) single nanohole (no standing current), three coupled nanoholes forming a linear dipole antenna.

that the nanoholes in a chain scatter light coherently. We treat the chain as an N-element linear array of uncoupled point dipoles and calculate the far-field emission patterns. Owing to the coherent far-field superposition of the scattered light emitted by the different dipoles, we expect a high directionality for large N. As shown in Fig. 5a, this is also the case: the lobes of the emission pattern for $N = 18$ are much narrower than that of a single dipole. The scattering from the chains becomes concentrated in a plane that contains the optical axis for the in-phase illumination configuration ($\theta = 180°$ in Fig. 5a), corresponding to an optimal collection efficiency and visibility. In the out-of-phase configuration, on the other hand, the chains are expected to beam the scattered light outside the collection angle of the objective (indicated as black solid lines in Fig. 5a), which makes them invisible in the dark-field microscope. What is surprising is that this 'beaming effect' is pronounced even when the number of participating dipoles is very small. Taking into account the complete three-dimensional projection of the radiation pattern on the solid angle of the objective for the $N = 3$ case in Fig. 5a, we estimate that ~40% of the scattered intensity will be lost in the case of out-of-phase illumination, compared with the collection efficiency for the in-phase case. From the electromagnetic reciprocity theory, we expect

that hole coupling will cause further enhancement of the emission directionality, similar to the excitation directionality found from equation (2). Together with the aforementioned decrease in effective polarizability for the out-of-phase illumination, the net result will be a drastic reduction in visibility even for short chains, as observed in the experiments.

On the basis of the analysis above, we can now interpret the variation in chain visibility seen in Fig. 1 as the combined result of two effects: (1) a high directionality of the chain emission pattern due to the coherent superposition of the fields emanating from each individual hole and (2) a remarkable sensitivity of the effective nanohole polarizability in a chain to the phase-dependent inter-hole coupling and incident polarization. As the net result of these processes is that the nanohole chains effectively behave as linear nano-optical antennas, it is interesting to draw an analogy with ordinary macroscopic antennas. As shown in Fig. 5b, the a_b SPP charge waves that emanate from a nanohole create a current distribution in the metal film analogous to that of a conventional linear wire antenna. We can qualitatively think of the nanohole as the feed of the antenna, whereas the surface charge waves act as the current distribution in the arms. A single hole, however, is not an antenna, because a standing wave cannot be created in the arms. Including more holes allows, on the one hand, a build-up of further charges in the arms and, on the other hand, it allows the charge waves emanating from one hole to be reflected from the edges of its nearest neighbours, leading to a standing current. It is well known from antenna theory that a high directionality can be obtained in a linear wire antenna if the length of each arm is equal to $\lambda/2$, where λ is the wavelength radiated by the antenna[35]. To obtain the equivalent current distribution in the thin gold film, the length of the arms must equal $\lambda_{SPP}/2$. The minimum number of holes that can form this type of linear antenna is clearly $N = 3$, which is where the invisibility phenomenon starts to become pronounced (see Supplementary Information for further experimental support of the antenna picture).

METHODS

FABRICATION

Linear chains of $N = 1$–18 circular nanoholes were milled in $t = 20$-nm-thick gold films using a focused ion beam (FEI Strata 235 Dual Beam). The thin gold films were thermally evaporated on SiO_2 glass slides using a 1 nm Ti adhesion layer. All nanoholes were $D \approx 70 \pm 10$ nm in diameter and the edge-to-edge distance was varied from $d = 30$ to 390 nm $\pm$ 5%. The inaccuracy in D and d, which is due to precision limitations of the focused ion beam, can result in variations in the nanohole resonance wavelength of the order of about 30 nm and can also affect the absolute intensities and intensity ratios between different illumination configurations, in particular for large N values. For example, it is likely that the extremely large enhancement of the scattering efficiency per hole observed for the $N = 3$ chain in Fig. 4b, compared with $N = 5$–18, reflects the difficulty in producing precise long chains rather than an intrinsic effect.

ELASTIC SCATTERING MEASUREMENTS

White light from a 100 W halogen lamp illuminates the sample from above at a fixed angle of incidence $\Phi = 62.5° \pm 10°$ (air condenser) or $\Phi = 60° \pm 8°$ (oil-immersion condenser) that exceeds the collection angle of the microscope objective ($\times 60$ air, NA = 0.7, or $\times 100$ oil, NA $\approx$ 1.0), which then channels the scattered light to a single-grating spectrometer (Shamrock SR-303i, Andor) equipped with a CCD (charge-coupled device) detector (iDus, Andor). A polarizer/slit-system placed directly above the dark-field condenser enables us to vary the polarization and the direction of the incident k vector relative to the nanohole chain axis.

FAR-FIELD RADIATION PATTERN SIMULATIONS

To mimic the experimental conditions of Fig. 4b, we fix the separation distance between dipoles at $d_{dip} = \lambda_{SPP}/2 + 2r$, where r is the radius of the nanohole. The polarization of the incident light is assumed to be parallel to the chain, its wavelength $\lambda_0 = 650$ nm, that is, at the peak of a typical scattering spectrum, and the angle of incidence is set to 60°. For the out-of-phase configuration, this set of parameters corresponds to a phase difference between neighbouring dipoles of $\phi \approx 0.6\pi$.

Received 2 February 2007; accepted 15 October 2007; published 18 November 2007.

References

1. Barnes, W. L., Dereux, A. & Ebbesen, T. W. Surface plasmon subwavelength optics. *Nature* **424**, 824–830 (2003).
2. Ozbay, E. Plasmonics: Merging photonics and electronics at nanoscale dimensions. *Science* **311**, 189–193 (2006).
3. Ebbesen, T. W., Lezec, H. J., Ghaemi, H. F., Thio, T. & Wolff, P. A. Extraordinary optical transmission through sub-wavelength hole arrays. *Nature* **391**, 667–669 (1998).
4. Maier, S. A. *et al.* Local detection of electromagnetic energy transport below the diffraction limit in metal nanoparticle plasmon waveguides. *Nature Mater.* **2**, 229–232 (2003).
5. Andrew, P. & Barnes, W. L. Energy transfer across a metal film mediated by surface plasmon polaritons. *Science* **306**, 1002–1005 (2004).
6. Bozhevolnyi, S. I., Volkov, V. S., Devaux, E. & Ebbesen, T. W. Channel plasmon-polariton guiding by subwavelength metal grooves. *Phys. Rev. Lett.* **95**, 046802 (2005).
7. Fromm, D. P., Sundaramurthy, A., Schuck, P. J., Kino, G. & Moerner, W. E. Gap-dependent optical coupling of single "Bowtie" nanoantennas resonant in the visible. *Nano Lett.* **4**, 957–961 (2004).
8. Muhlschlegel, P., Eisler, H. J., Martin, O. J. F., Hecht, B. & Pohl, D. W. Resonant optical antennas. *Science* **308**, 1607–1609 (2005).
9. Xu, H. X., Bjerneld, E. J., Kall, M. & Borjesson, L. Spectroscopy of single hemoglobin molecules by surface enhanced Raman scattering. *Phys. Rev. Lett.* **83**, 4357–4360 (1999).
10. Mirkin, C. A., Letsinger, R. L., Mucic, R. C. & Storhoff, J. J. A DNA-based method for rationally assembling nanoparticles into macroscopic materials. *Nature* **382**, 607–609 (1996).
11. Haes, A. J., Chang, L., Klein, W. L. & Van Duyne, R. P. Detection of a biomarker for Alzheimer's disease from synthetic and clinical samples using a nanoscale optical biosensor. *J. Am. Chem. Soc.* **127**, 2264–2271 (2005).
12. Rindzevicius, T. *et al.* Plasmonic sensing characteristics of single nanometric holes. *Nano Lett.* **5**, 2335–2339 (2005).
13. Pendry, J. B. Negative refraction makes a perfect lens. *Phys. Rev. Lett.* **85**, 3966–3969 (2000).
14. Shelby, R. A., Smith, D. R. & Schultz, S. Experimental verification of a negative index of refraction. *Science* **292**, 77–79 (2001).
15. Dolling, G., Enkrich, C., Wegener, M., Soukoulis, C. M. & Linden, S. Simultaneous negative phase and group velocity of light in a metamaterial. *Science* **312**, 892–894 (2006).
16. Zhang, S. *et al.* Experimental demonstration of near-infrared negative-index metamaterials. *Phys. Rev. Lett.* **95**, 137404 (2005).
17. Lezec, H. J. *et al.* Beaming light from a subwavelength aperture. *Science* **297**, 820–822 (2002).
18. Degiron, A. & Ebbesen, T. W. The role of localized surface plasmon modes in the enhanced transmission of periodic subwavelength apertures. *J. Opt. Pure Appl. Opt.* **7**, S90–S96 (2005).
19. Grupp, D. E., Lezec, H. J., Thio, T. & Ebbesen, T. W. Beyond the Bethe limit: Tunable enhanced light transmission through a single sub-wavelength aperture. *Adv. Mater.* **11**, 860–862 (1999).
20. Ruan, Z. C. & Qiu, M. Enhanced transmission through periodic arrays of subwavelength holes: The role of localized waveguide resonances. *Phys. Rev. Lett.* **96**, 233901 (2006).
21. van der Molen, K. L. *et al.* Role of shape and localized resonances in extraordinary transmission through periodic arrays of subwavelength holes: Experiment and theory. *Phys. Rev. B* **72**, 045421 (2005).
22. Treacy, M. M. J. Dynamical diffraction explanation of the anomalous transmission of light through metallic gratings. *Phys. Rev. B* **66**, 195105 (2002).
23. Vigoureux, J. M. Analysis of the Ebbesen experiment in the light of evanescent short range diffraction. *Opt. Commun.* **198**, 257–263 (2001).
24. Lezec, H. J. & Thio, T. Diffracted evanescent wave model for enhanced and suppressed optical transmission through subwavelength hole arrays. *Opt. Express* **12**, 3629–3651 (2004).
25. Gay, G. *et al.* The optical response of nanostructured surfaces and the composite diffracted evanescent wave model. *Nature Phys.* **2**, 262–267 (2006).
26. Burke, J. J., Stegeman, G. I. & Tamir, T. Surface-polariton-like waves guided by thin, lossy metal-films. *Phys. Rev. B* **33**, 5186–5201 (1986).
27. Rindzevicius, T. *et al.* Nanohole plasmons in optically thin gold films. *J. Phys. Chem. C* **111**, 1207 (2007).
28. Prikulis, J., Hanarp, P., Olofsson, L., Sutherland, D. & Kall, M. Optical spectroscopy of nanometric holes in thin gold films. *Nano Lett.* **4**, 1003–1007 (2004).
29. Hanarp, P., Kall, M. & Sutherland, D. S. Optical properties of short range ordered arrays of nanometer gold disks prepared by colloidal lithography. *J. Phys. Chem. B* **107**, 5768–5772 (2003).
30. Draine, B. T. & Flatau, P. J. Discrete-dipole approximation for scattering calculations. *J. Opt. Soc. Am. A* **11**, 1491–1499 (1994).
31. Gunnarsson, L. *et al.* Confined plasmons in nanofabricated single silver particle pairs: Experimental observations of strong interparticle interactions. *J. Phys. Chem. B* **109**, 1079–1087 (2005).
32. Gao, H. W., Henzie, J. & Odom, T. W. Direct evidence for surface plasmon-mediated enhanced light transmission through metallic nanohole arrays. *Nano Lett.* **6**, 2104–2108 (2006).
33. Chang, S. H., Gray, S. K. & Schatz, G. C. Surface plasmon generation and light transmission by isolated nanoholes and arrays of nanoholes in thin metal films. *Opt. Express* **13**, 3150–3165 (2005).
34. Sepulveda, B., Lechuga, L. A. & Armelles, G. Magnetooptic effects in surface-plasmon-polaritons slab waveguides. *J. Lightwave Technol.* **24**, 945–955 (2006).
35. Balanis, C. A. *Antenna Theory: Analysis and Design* (Wiley, New Jersey, 2005).

Acknowledgements

The authors thank P. Johansson, J. G. de Abajo, J. Aizpurua, P. Nordlander, T. Rindzevicius, T. Pakizeh and S. A. Astakhov for stimulating discussions and suggestions. Financial support from the Swedish Research Council and the Swedish Foundation for Strategic Research is gratefully acknowledged. Correspondence and requests for materials should be addressed to Y.A. or M.K. Supplementary Information accompanies this paper on www.nature.com/naturephysics.

Author contributions

Y.A. and L.E. prepared the samples. Y.A. and B.S. carried out optical measurements and data analysis. B.S. and M.K. made numerical simulations and analytical theory. Y.A., B.S., E.O. and M.K. planned the work. Y.A., B.S. and M.K. wrote the paper. All authors discussed the results.

Supplementary Information

1. Scattering intensities versus *d* for N = 3 and perpendicular polarization

When the polarization of the incoming light is perpendicular to the chain, the weak interaction between the nanoholes prevents a large amplification of the effective polarizability for in phase illumination, see Fig. S1a. However, the "beaming" effect is still pronounced for d < ~400 nm, as indicated by the reduction in intensity seen in Fig. S1a for the out-of-phase configuration and the directional radiation lobes calculated for three dipoles oriented perpendicular to the chain in Fig. S1b. This explains why a large contrast between the in-phase and out-of-phase configurations is seen even for unpolarized incident light, as illustrated in Fig. 1.

2. Images and spectra collected using oil-immersion optics

Figure S2a display dark-field images of N = 3, 8 and 18 chains for polarization parallel to the chains. The images were collected using oil immersion optics to improve contrast further and to allow for a ~15% increase in collection angle. In the case of N = 3 and d = 150 nm (Fig. S2a-I), the chain appears as a single intense red spot for *in-phase* illumination (top row). In the antenna analogy, we can interpret the bright spot as the feed of the antenna. For out-of-phase illumination (bottom row), on the other hand, we see two weak reddish spots corresponding to the outer edges of the two outermost holes, i.e. regions that are not part of the linear antenna. For long separation distances (d > 400nm) and weak coupling, in contrast, all three holes are clearly seen with similar intensity in both configurations (Fig. S2a-II). If we

now increase the length of the chain to N = 8 or 18 for d = 150 nm (Fig. S2a-III, IV) we see that the bright and homogeneous red lines that dominate for in phase illumination are matched by equal length weak green lines flanked by two reddish spots in the out-of-phase case. Fig. S2b shows a spectral analysis of the *central* part of the N = 18 chain. It is clear that the green colour is a consequence of a lack of “red” light in the scattering spectrum. The spectral region that is depleted (λ = 600 – 700 nm) matches the position of the chain resonance observed for the *in-phase* illumination condition, as well as the single hole resonance position, (see Fig. 4b) and gives further support to the idea that the visibility contrast originates in a strong SPP induced hole interaction in conjunction with a high directionality due to far-field interference between individual hole scatterers.

FIGURE CAPTIONS (Supplementary Information)

Figure S1. Experimental results and modelling for the case of the polarization perpendicular to a *N* = 3 nanohole chains. **a,** Experimental elastic scattering intensity dependence on the edge-to-edge distance between nanoholes (*d*). **b**, Simulated far-field emission patterns for *N* = 3 uncoupled dipoles oriented perpendicular to the chain.

Figure S2. Images and spectrum measured using oil immersion optics a, Dark-field microscopy images of linear chains of nanoholes in the *in-phase* (top row) and the *out-of-phase* configurations (bottom row), **I**: N=3, $d \approx \lambda_{SPP}/2$; **II**: N=3, $d \approx 2 \cdot \lambda_{SPP}$; **III**: N=8, $d \approx \lambda_{SPP}/2$; **IV**: N=18, $d \approx \lambda_{SPP}/2$. **b**, Elastic scattering spectrum measured from the central part (green) of the N = 18 (IV, bottom row) chain in the *out-of-phase* configuration.

Figure S1

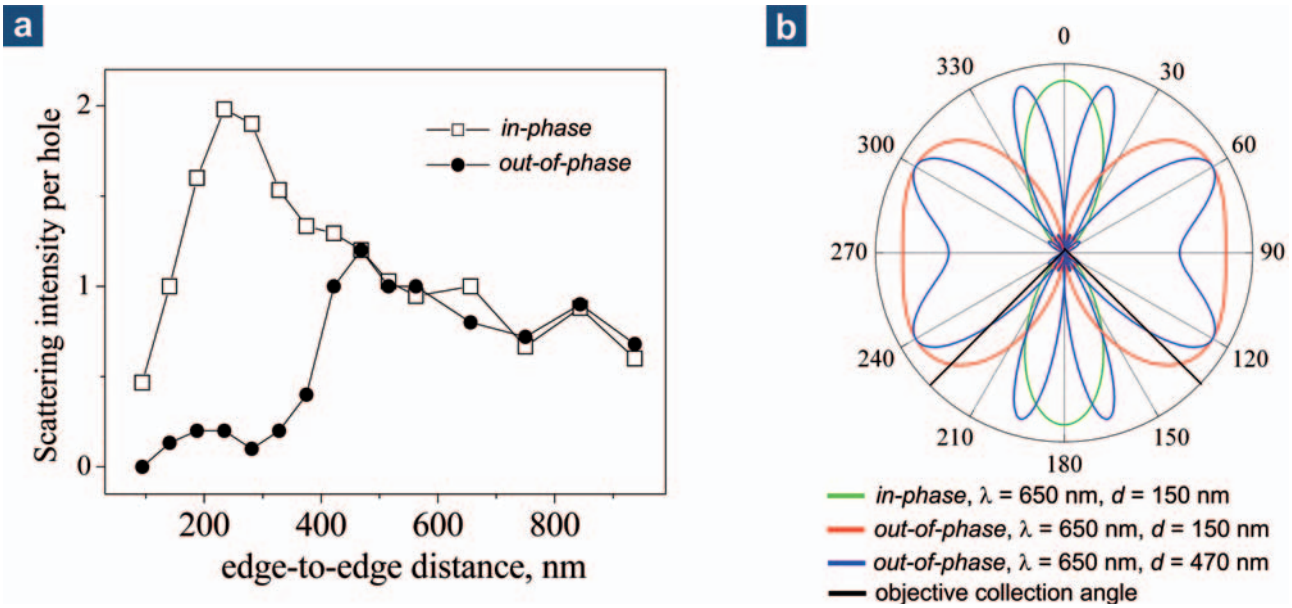

Figure S2